*J. Fluid Mech.* (1997), *vol.* 332, *pp.* 105–120



# Absolute and convective instability of a viscous liquid curtain in a viscous gas

By C. H. TENG, S. P. LIN AND J. N. CHEN

Department of Mechanical and Aeronautical Engineering, Clarkson University, Potsdam, NY 13699, USA

(Received 31 October 1995 and in revised form 6 June 1996)

The linear instability of a viscous liquid flowing in a vertical sheet sandwiched between two viscous gases bounded externally by two vertical walls is investigated. The critical Weber number below which the flow is absolutely unstable and above which the flow is convectively unstable is found to be approximately equal to one and is weakly dependent on the rest of the parameters. The Weber number is defined as $We \equiv \rho_1 U_0^2 d/S$ where $S$ is the surface tension, $\rho_1$ is the liquid density, $U_0$ is the centre-line velocity of the liquid sheet, and $d$ is the half-thickness of the uniform liquid sheet. The sinuous mode is found to have a greater amplification rate than the varicose mode in the convective instability regime. While absolute instability is caused by the surface tension, convective instability is caused by the amplification of disturbances near the liquid–gas interface. The surface tension, and viscosities of liquids and gases all suppress the amplification of the convectively unstable disturbances. An increase in the gravitational force or the gas density results in an enhancement of the amplification rate.

## 1. Introduction

The dynamics of thin sheets of liquids was investigated by Taylor (1959*a–c*). The disintegration of liquid sheets in the context of atomization has been studied by Clark & Dombrowski (1972), Crapper *et al.* (1973), Crapper, Dombrowski & Pyott (1975) and Weihs (1978). Brown (1961), Lin (1981) and Lin & Roberts (1981) studied the stability of liquid sheets formed by extrusion. A thin sheet of viscous liquids flowing between two vertical guide wires is an integral part of curtain coating processes used widely in various applications. Kistler & Scriven (1984) investigated the curtain coating flow numerically by use of finite-element methods. Some description of this process and its applications in various industries can be found in the references cited above. Lin predicted the wave speeds of two distinctive modes of disturbances which exhibit themselves in the form of sinuous and varicose waves. In sinuous waves the two free surfaces of a liquid curtain are displaced in phase, and in varicose waves the two surfaces are displaced in the opposite direction along the axis. These waves were observed by Lin & Roberts (1981) and Antoniades & Lin (1980). They also exploited the wave properties to experimentally determine the value of dynamic surface tension on a rapidly moving free surface.

In the theoretical works cited above, the effect of the ambient gas is completely neglected. On the other hand, all of the experiments cited above were carried out in the presence of the ambient gas. This prompted Lin, Lian & Creighton (1990) to study the effect of the ambient gas. They found that the ambient gas is destabilizing, and tends to shorten the sinuous as well as the varicose waves. This is consistent with the results

of Taylor (1963) who showed that the ambient gas tends to shorten the wavelength of ripples formed on a viscous liquid. They also found that the liquid sheet is convectively unstable if the ratio of the surface tension force to the inertial force per unit interfacial area is smaller than one. When this ratio is greater than one, they predicted that the liquid sheet is neutral. On the other hand, Lin & Roberts (1981) and Antoniades & Lin (1980) observed that when this ratio is greater than one, the liquid sheet ruptures explosively. This apparent inconsistency may be due to the fact that the basic flow suggested by Taylor and used by Lin *et al*. is not an exact solution of the Navier–Stokes equation and that the viscosity of the ambient gas is neglected.

Here we investigate the absolute and convective instability of a viscous liquid sheet flowing in a viscous gas. This basic flow satisfies the Navier–Stokes equations exactly. The problem formulated in §2 is solved by use of the spectral method described in §3. The numerical results given in §4 delineate the effects of all relevant flow parameters on the absolute and convective instability, both of which are found. Huerre & Monkewitz (1985) demonstrate that a counterflow in free shear layers tends to promote absolute instability. In the limit of an infinitely large Reynolds number, they show that if the counterflow velocity is greater than 13.6% of main stream velocity absolute instability will occur. The present exact basic flows include flows with and without counterflows. Absolute instability is found for both flows. It is demonstrated that the absolute instability in a liquid curtain is caused by the surface tension. Leib & Goldstein (1986*a*, *b*) were the first to demonstrate that absolute instability can be produced by surface tension effects. The present results show that absolute instability does occur when the Weber number is approximately one as observed by Antoniades & Lin (1980). The practical implications and the theoretical significance of the obtained results are discussed in the last section.

## 2. Formulation of the problem

Consider the stability of a viscous liquid sheet of constant thickness $2d$. The liquid sheet is surrounded by a viscous gas which is bounded by two vertical walls located at equidistance $L$ from the centreline of the liquid sheet. For the liquid sheet to maintain a constant thickness, the pressure gradient in the liquid- and gas-flows must remain constant. In the presence of gravity, such parallel flows of incompressible liquid and gas which satisfy the Navier–Stokes equations are given by

$$U_i = \tfrac{1}{2}K_i y^2 \pm A_i y + B_i \quad (i = 1, 2), \tag{1}$$

where $U$ is the velocity normalized with the centreline velocity of the liquid sheet $U_0$ in the direction of gravitational acceleration, the subscript $i$ stands for the liquid or the gas phase depending if it is 1 or 2, $y$ is the horizontal distance measured from the centreline to the right divided by $d$, and $+$ or $-$ signs in front of $A_i$ are the domain $1 \leqslant y \leqslant 1+l$ or $-1-l \leqslant y \leqslant -1$ respectively, $l$ being $(L-d)/d$. The integration constants $A_i$ and $B_i$, and $K_i$ which are related to the dynamic pressure gradient are given by

$$\begin{aligned}
&K_1 = Re\,(K - Fr), \quad A_1 = 0, \quad B_1 = 1,\\
&K_2 = (Re/\mu_r)\,(K - \rho_r Fr), \quad A_2 = (K_1/\mu_r - K_2),\\
&B_2 = -K_2(1+l)^2/2 - (K_1/\mu_r - K_2)\,(1+l),\\
&K = Fr\,(\mu_r + 2l + \rho_r l^2)/(\mu_r + 2l + l^2) - 2\mu_r/[Re\,(\mu_r + 2l + l^2)],
\end{aligned}$$

where

$$\begin{aligned}
Re &\equiv \text{Reynolds number} = \rho_1 U_0 d/\mu_1,\\
Fr &\equiv \text{Froude number} = gd/U_0^2,\\
\mu_r &= \mu_2/\mu_1, \quad \rho_r = \rho_2/\rho_1, \quad l = (L-d)/d.
\end{aligned}$$

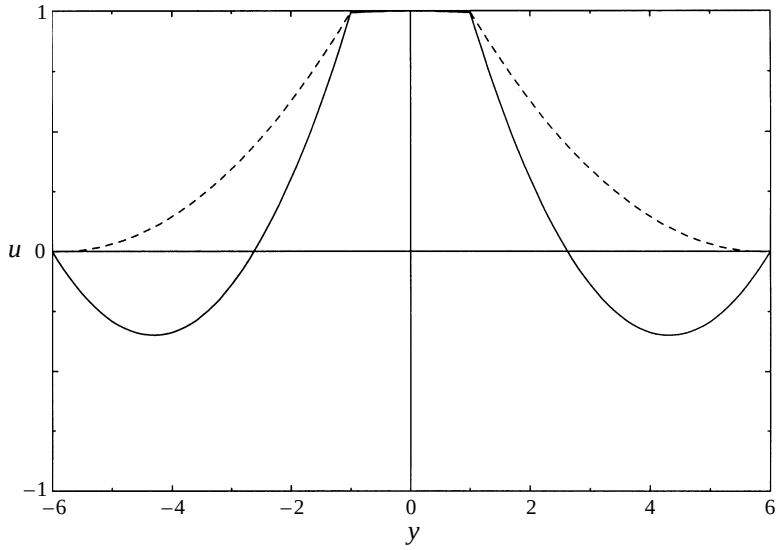


FIGURE 1. Basic flow velocity profile, $Re = 52.72$, $\rho_r = 0.0013$, $\mu_r = 0.017$, $l = 5$: ——, $Fr = 0.00340625$; – – –, 0.00016.

Some representative velocity distributions are given in figure 1. Note that the gas flow may or may not have counter flows depending on the flow parameters. The values of $\rho_r$ and $\mu_r$ given in this figure correspond to a water curtain in air at 1 atm. pressure and 20 °C.

The stability of the basic state described by (1) with respect to a normal mode two-dimensional disturbance is governed by the well known Orr–Sommerfeld equation (Drazin & Reid 1985),

$$\left.\begin{aligned} &[\omega-(N_i'/Re)\,\mathrm{D}^2]\,\mathrm{D}^2\phi_i(y)+\mathrm{i}kU_i\,\mathrm{D}^2\phi_i-\mathrm{i}k(\mathrm{d}^2U_i)\,\phi_i=0,\\ &\mathrm{D}^2=\mathrm{d}^2-k^2,\quad \mathrm{d}^2=\mathrm{d}^2/\mathrm{d}y^2,\quad N_i'=\nu_i/\nu_1, \end{aligned}\right\} \tag{2}$$

where $\nu$ is the kinematic viscosity, $\omega = \omega_r + \mathrm{i}\omega_i$ and $k = k_r + \mathrm{i}k_i$ are, respectively, the dimensionless complex frequency and the wavenumber of the disturbance, and $\phi_i$ is the amplitude of the normal mode disturbance related to the Stokes stream function $\psi_i$ by

$$\psi_i(x, y, t) = \phi_i(y)\,\mathrm{e}^{(\mathrm{i}kx+\omega t)}, \tag{3}$$

where $t$ is time normalized with $d/U_0$, and $x$ is the distance measure in the unit of $d$ in the liquid flow direction from the origin of the Cartesian coordinate $(x, y)$. The Stokes stream function is related, respectively, to the $x$- and $y$-components of the disturbance velocity by

$$u_i = \psi_{i,y}, \quad v_i = -\psi_{i,x},$$

where the subscripts $x$ and $y$ denote partial differentiations.

The boundary conditions at the perturbed liquid–gas interfaces can be linearized by use of the Taylor series expansions of all variables involved about $y = \pm 1$, and retaining only terms of the first order in perturbations. Hence, the interfacial conditions are to be evaluated at $y = \pm 1$ with the corresponding interfacial displacements $\eta_\pm$ as additional unknowns. Since the interface is a material surface, $\eta_\pm$ must satisfy at $y = \pm 1$ the kinematic condition

$$\eta_{\pm,t} + U_1\,\eta_{\pm,x} = -\psi_{1,x}.$$

Other interfacial kinematic conditions are the continuity of the $y$- and $x$-components of the velocity across the interfaces given respectively by

$$[\psi_{i,x}]_2^1 = [\psi_{1,x} - \psi_{2,x}]_{y=\pm 1} = 0, \quad [\psi_{i,y} + U_{i,y}\,\eta_\pm]_2^1 = 0,$$

where $\eta_+$ or $\eta_-$ is to be used for the boundary conditions at $y = 1$ or $-1$. The balancing of forces per unit area of the interface in the tangential and normal directions leads, respectively, to the dynamic conditions at $y = \pm 1$,

$$[M_i(\eta_\pm\, U_{i,yy} + \psi_{i,yy} - \psi_{i,xx})]_2^1 = 0,$$
$$[p_i + (2/Re)\, M_i\, \psi_{i,xy}]_2^1 \pm We^{-1}\eta_{\pm,xx} = 0,$$

where $p_i$ is the perturbation pressure,

$$We \equiv \text{Weber number} \equiv \rho_1\, U_0^2\, d/S, \quad M_i = \mu_i/\mu_1.$$

Thus, $We$ signifies the ratio of the inertial force to the surface tension force per unit area of the interface. The boundary conditions at the walls $y = \pm(1+l)$ are

$$\psi_{2,x} = 0, \quad \psi_{2,y} = 0.$$

The normal mode pressure and interfacial displacement are written as

$$[p_i, \eta_\pm] = [\zeta_i(y), \xi_\pm]\, \mathrm{e}^{(\mathrm{i}kx + \omega t)}. \tag{4}$$

Substituting (1), (3) and (4) into the above boundary conditions, we rewrite them in the same order of appearance

$$\mathrm{i}k\phi_1 + [\omega + \mathrm{i}kU_1]\,\xi_\pm = 0, \tag{5a}$$
$$[\phi_i]_2^1 = 0, \tag{5b}$$
$$[\phi_{i,y} + \xi_\pm\, U_{i,y}]_2^1 = 0, \tag{5c}$$
$$[M_i\{(\mathrm{d}^2 + k^2)\,\phi_i + U_{i,yy}\,\xi_\pm\}]_2^1 = 0, \tag{5d}$$
$$[\zeta_i + (2\mathrm{i}k/Re)\, M_i\, \phi_{i,y}]_2^1 \mp k^2 We^{-1}\xi_\pm = 0, \tag{5e}$$
$$\phi_2[\pm(1+l)] = 0, \tag{5f}$$
$$\phi_{2,y}[\pm(1+l)] = 0. \tag{5g}$$

The pressure amplitude discontinuity in (5$e$) can be obtained from the linearized Navier–Stokes equations, and is found to be

$$(-\mathrm{i}k)\,[\zeta_i]_2^1 = [Q_i\{(\omega + \mathrm{i}kU_i)\,\phi_{i,y} - \mathrm{i}kU_{i,y}\,\phi_i\} - M_i\,\mathrm{D}^2\phi_{i,y}/Re]_2^1.$$

where $Q_i = \rho_i/\rho_1$.

Non-trivial solutions of (2) with its boundary conditions (5$a$)–(5$g$) for given flow parameters $Re$, $Fr$, $We$, $\rho_r$, $\mu_r$, $l$ and $k$ exist only for certain eigenvalues $\omega$. The real and imaginary parts of $\omega$ give, respectively, the temporal growth rate and the frequency corresponding to the real wavenumber $k_r$, and the spatial amplification rate $k_i$.

## 3. Solution by Chebyshev expansion

The solution of the formulated problem will be expanded in Chebyshev polynomials. The gas domains $y \epsilon [1, 1+l]$ and $y \epsilon [-1-\lambda, -1]$ are mapped into $y_+ \epsilon [-1, 1]$ and $y_- \epsilon [-1, 1]$, respectively, by use of the linear transformations

$$y = 1 - \tfrac{1}{2}l(y_+ - 1), \quad y = -1 - \tfrac{1}{2}l(y_- + 1).$$

| $N_1$ | $N_2$ | $\omega_r$ | $-\omega_i$ |
|---|---|---|---|
| 15 | 30 | 0.01668370 | 4.71282368 |
| 20 | 40 | 0.01487745 | 4.71166567 |
| 30 | 62 | 0.01477907 | 4.71171634 |
| 31 | 64 | 0.01477890 | 4.71171627 |
| 32 | 66 | 0.01477908 | 4.71171503 |
| 33 | 68 | 0.01478001 | 4.71171482 |
| 34 | 70 | 0.01478024 | 4.71171521 |
| 35 | 72 | 0.01478075 | 4.71171620 |

TABLE 1. Chebyshev approximation for $Re = 15711.77$, $Fr = 7.67 \times 10^{-6}$, $We = 8880.9947$, $\rho_r = 0.0013$, $\mu_r = 0.017$, $l = 5.0$, $k_r = 5.0$, $k_i = 0$

In the new variables $y_\pm$, the expressions of the Orr–Sommerfeld equation and its boundary conditions remain the same except the $n$th derivatives appearing in these equations must be multiplied by $(-2/l)^n$, and the basic flow in the gas region is written as

$$U_{2\pm} = Ey_\pm^2 \pm Fy_\pm + H, \tag{6}$$

where
$$E = (K_2 l^2/8), \quad F = -[l(1+l/2)\,K_2/2 + lA_2/2],$$
$$H = (1+l+l^2/4)\,K_2/2 + (1+l/2)\,A_2 + B_2.$$

The corresponding perturbation amplitude can be expanded in the series of Chebyshev polynomials of $n$th degree

$$\left.\begin{aligned} \phi_1(y) &= \sum_{n=0}^{N} a_n\, T_n(y) \quad (-1 \leqslant y \leqslant 1), \\ \phi_{2+}(y_+) &= \sum_{n=0}^{N_2} b_n\, T_n(y_+) \quad (-1 \leqslant y_+ \leqslant 1), \\ \phi_{2-}(y_-) &= \sum_{n=0}^{N_2} c_n\, T_n(y_-) \quad (-1 \leqslant y_- \leqslant 1). \end{aligned}\right\} \tag{7}$$

By substituting (7) into the Orr–Sommerfeld equation and performing the Galerkin projection with $T_m$, where $0 \leqslant m \leqslant N$ in liquid domain and $0 \leqslant m \leqslant N_2$ in each gas domain, we obtain $N+1$ equations in liquid domain, and $N_2+1$ equations in each gas domain. The Galerkin projections of $\phi_1, \phi_{2\pm}$ as well as their derivatives and their products with powers of $y$ and $y_\pm$ can also be expanded in series of Chebyshev polynomials in each domain. Since the Orr–Sommerfeld equation in terms of $a_n$ is available in the literature (Orszag 1971; Gottlieb & Orszag 1977) and that in terms of $b_n$ or $c_n$ has the same expressions except with an additional term arising from $Fy_\pm$ in the basic flow (6), they will not be given here.

Since the governing system of equations is linear and homogeneous, the solution can be separated into even and odd functions of $y$. For the even solution, $\phi_1(1) = \phi_1(-1)$. It follows from (5*a*) that $\xi_+ = \xi_- = \xi$, since $U_1(1) = U_1(-1)$. The displacements at the two liquid–gas interfaces are in phase for the even solution which will therefore be termed the sinuous mode. For the odd solution, $\phi_1(1) = -\phi_1(-1)$ and $U_1(1) = U_1(-1)$, and therefore it follows from (5*a*) that $\xi_+ = -\xi_-$. Hence the odd solution will be termed varicose mode. The even and odd solutions are decoupled.

For the sinuous mode, we retain only the even Chebyshev polynomials in $\phi_1$. Using the relation $T_n(\pm 1) = (\pm 1)^n$ the corresponding boundary conditions at $y = y_+ = 1$ are written as

$$[\omega + \mathrm{i}kU_1(1)]\,\xi + \mathrm{i}k \sum_{n=0}^{N_1} a_{2n} = 0, \tag{8a}$$

$$\sum_{n=0}^{N_1} a_{2n} - \sum_{n=0}^{N_2} b_n = 0, \tag{8b}$$

$$[U_{1,y} - U_{2,y}]\,\xi + \sum_{n=0}^{N_1} (2n)^2 a_{2n} + (2/l) \sum_{n=0}^{N_2} n^2 b_n = 0, \tag{8c}$$

$$\sum_{n=0}^{N_1} [4n^2(4n^2-1)/3 + k^2]\, a_{2n} - \mu_r \sum_{n=0}^{N_2} [(2/l)^2 n^2(n^2-1)/3 + k^2]\, b_n + (U_{1,yy} - \mu_r U_{2,yy})\,\xi = 0, \tag{8d}$$

$$\sum_{n=0}^{N_1} \left[ -\left(\frac{3k^2}{Re} + \mathrm{i}kU_1\right)(4n^2) + \mathrm{i}kU_{1,y} + (2n)^2(4n^2-1)(4n^2-4)/(15Re) - \omega(2n)^2 \right] a_{2n} - \sum_{n=0}^{N_2} \left[ \mathrm{i}k(3\mathrm{i}k\mu_r/Re - U_2\rho_r)\left(-\frac{2}{l}\right) n^2 + \mathrm{i}kU_{2,y}\rho_r + \mu_r \left(-\frac{2}{l}\right)^3 n^2(n^2-1) \times (n^2-4)/(15Re) - \omega\rho_r \left(-\frac{2}{l}\right) n^2 \right] b_n - \mathrm{i}k^3 We^{-1}\xi = 0, \tag{8e}$$

$$\sum_{n=0}^{N_2} (-1)^n b_n = 0, \tag{8f}$$

$$\sum_{n=0}^{N_2} (-1)^{n+1} n^2 b_n = 0. \tag{8g}$$

For the varicose mode, the system of equations remains the same except that the $a_{2n+1}$ terms are retained in the expansions of $\phi_1$.

The unknowns of the system are $\xi, b_n$ ($n = 0$ to $N_2$) and $a_{2n}$ or $a_{2n+1}$ ($n = 0$ to $N_1$) depending on whether one is dealing with the sinuous or varicose mode. To render the number of equations the same as the number of unknowns ($N_1 + N_2 + 3$), we used the method of Lanczos (1956) to truncate the Galerkin projection of the Orr–Sommerfeld equation. We chose $0 \leqslant m \leqslant N_1 - 2$ for the liquid domain and $0 \leqslant m \leqslant N_2 - 4$ for the gas domain. Hence the seven equations from the boundary conditions and the $N_1 + N_2 - 4$ equations from the Orr–Sommerfeld equations allow us to determine the eigenvector up to an arbitrary multiplication factor for each eigenvalue of the system if the flow parameters are given.

We use the method of Briggs (1964) and Bers (1983) to delineate the regime of absolute and convective instability in the parameter space. For a given set of ($Re$, $We$, $Fr, \mu_r, \rho_r, l$), $k_i$ is varied for each assigned value of $k_r$ to determine a corresponding set $(\omega_r, \omega_i)$ by use of the IMSL subroutine dg2ccg (see Rombers 1984). Recall that $k_i < 0$ gives the spatial growth rate of the disturbance. As $k_i$ is decreased from $k_i > 0$ to $k_i < 0$, the corresponding $\omega_r$ may decrease from some positive value $\omega_r > 0$ to $\omega_r < 0$. If this occurs over a finite range of $k_r$, and if the determinant, $D$, of the coefficient matrix of the homogeneous system is single valued and has only isolated singularities and $D^{-1} \to 0$ as $k_r \to \infty$ at least as fast as $k_r^{-1}$, then superposition of the normal modes by use of

the Fourier–Laplace integral represents the general disturbance which decays in time at a given location $x$ but grows in time as it is convected downstream with the group velocity $V_g = -\mathrm{d}\omega_i/\mathrm{d}k_r > 0$. Moreover, near $\omega_r = +0$, the causality condition that no disturbances grow in time at all $x$ when $t < 0$ is satisfied. The plot of $k_i$ *vs.* $k_r$ at $\omega_r = 0$ then gives the spatial amplification curve for the convectively unstable disturbance, the amplitude of which $G$ has a large-time asymptotic behaviour

$$G \sim t^{-1/2} \exp\left[-k_i(\omega_s)\, V_g\, t\right], \tag{9}$$

as seen by an observer travelling at $V_g$. In (9), $-k_i(\omega_s)$ is the maximum of $-k_i$, occurring at the real value of $\omega = \omega_s$.

However, in some parameter ranges, saddle-point singularities of $D^{-1}$ appear in the $k_r - k_i$ plane before $\omega_r$ is reduced to zero, as described above for the case of convective instability when $k_i < 0$. Then the large-time asymptotic behaviour of the disturbance is

$$G \sim t^{-1/2} \exp\left(-\mathrm{i}k_0\, x + \omega_0\, t\right), \tag{10}$$

where $k_0$ and $\omega_0$ are, respectively, the saddle-point and the branch-pole singularities in the $k$- and $\omega$-planes.

It is seen from (10) that the disturbance grows in time at any location $x > 0$, and the flow is absolutely unstable. Numerical results show that both instabilities occur in the present flow.

To test the possible syntax and computer program errors, the results for the special cases included in the present problem are checked against the known results of plane Poiseulle flow (Orszag 1971) and the temporal instability results of Renardy (1987). The numbers of terms retained in $\phi_1$ and $\phi_{2\pm}$ are systematically increased until five significant digits are obtained for the eigenvalue. A typical example of the convergence test is given in table 1.

## 4. Results and discussion

The spatial amplification curves for convectively unstable varicose disturbances are given in figure 2 for various values of *We* and the set of other flow parameters specified in the caption. Along these curves, $\omega_i$ decreases with $k_r$, and thus the packet of disturbances is convected in the downstream direction. It is seen that the amplification rate decreases as *We* is decreased. The converse is true for the sinuous mode with the same set of flow parameters, as shown in figure 3. Note that $-k_i$ of the sinuous mode is two orders of magnitude larger than that of the varicose model. The convectively unstable sinuous mode becomes absolutely unstable when *We* is decreased slightly below the smallest Weber number given in this figure. The emergence of a saddle point when *We* is reduced to 1, while the rest of the flow parameters remain the same as in the caption of figure 3, is shown in figure 4. The wave frequency of the saddle point lies between 0.014 and 0.0145. Two sets of curves of the same $\omega_i$ are shown in this figure. A member of each set originates from $k_i < 0$, and the other member from $k_i > 0$. Both members originates with $\omega_r > 0$. As $\omega_r$ is decreased toward zero, each member of the same set approaches a different branch of $\omega_r = 0$. Along the branch with larger wavenumbers $\mathrm{d}\omega_i/\mathrm{d}k_r > 0$, and along the other branch $\mathrm{d}\omega_i/\mathrm{d}k_r < 0$. Hence, the disturbances propagate upstream as well as downstream as they grow in time asymptotically according to (10). The transition from convective instability to absolute instability occurs at $We = 1.01$ for the flow specified by the parameters given in the caption of figures 2 or 3. An example of the transition Weber number as a function of

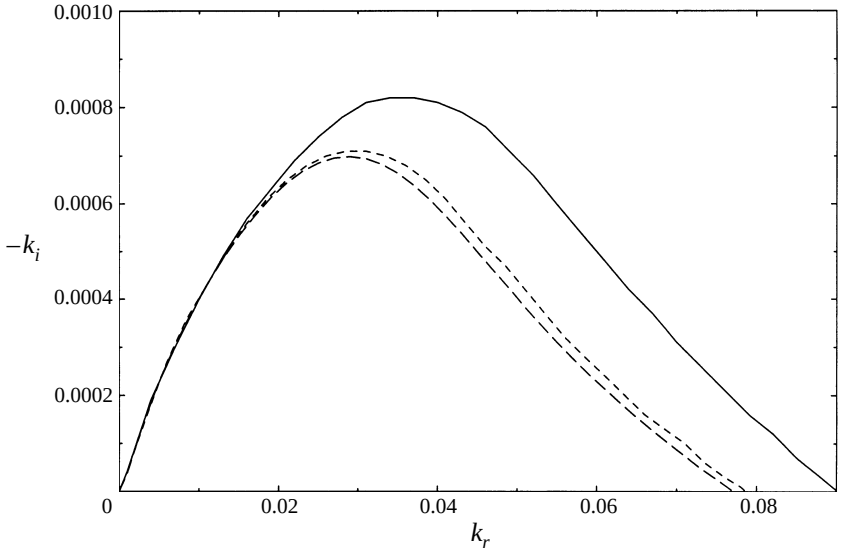


FIGURE 2. Varicose mode amplification rate. $Re = 52.72$, $Fr = 3.40625 \times 10^{-4}$, $\rho_r = 0.0013$, $\mu_r = 0.017$, $l = 5$: ——, $We = 2.0$; – – –, 1.1111; — —, 1.0204.

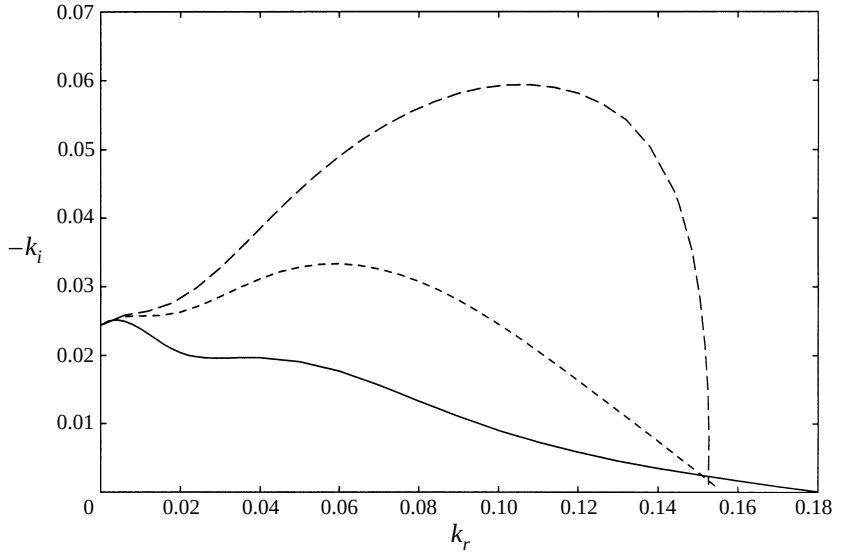


FIGURE 3. Sinuous mode amplification rate, $Re = 52.72$, $Fr = 3.40625 \times 10^{-4}$, $\rho_r = 0.0013$, $\mu_r = 0.017$, $l = 5$: ——, $We = 2.0$; – – –, 1.1111; — — —, 1.0204.

$Re$ is given in figure 5. The transition curve ($We_c$, $Re$) shown in figure 5 corresponds to the basic flows with counter flows similar to that shown by solid lines in figure 1. Huerre & Monkewitz (1985) demonstrated that, in the limit of $Re \to \infty$, if the velocity of the counterflow is greater than 13.6% of the mainstream velocity in free shear layers absolute instability will occur. However, the absolute instability reported here is not due to counterflows, since the absolute instability can be changed to convective instability by increasing the Weber number above $We_c$ without reducing the maximum velocity of the counterflow. In fact the basic flow without counterflow as shown in the dashed line in figure 1 can become absolutely unstable when $We$ becomes smaller than

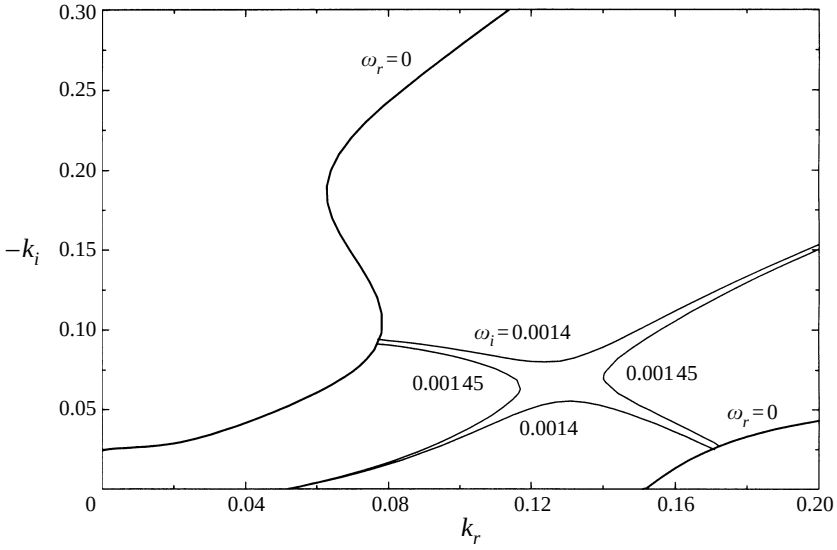


FIGURE 4. Saddle point in $k$-plane. $Re = 52.72$, $Fr = 3.40625 \times 10^{-4}$, $\rho_r = 0.0013$, $\mu_r = 0.017$, $l = 5$, $We = 1.0$.

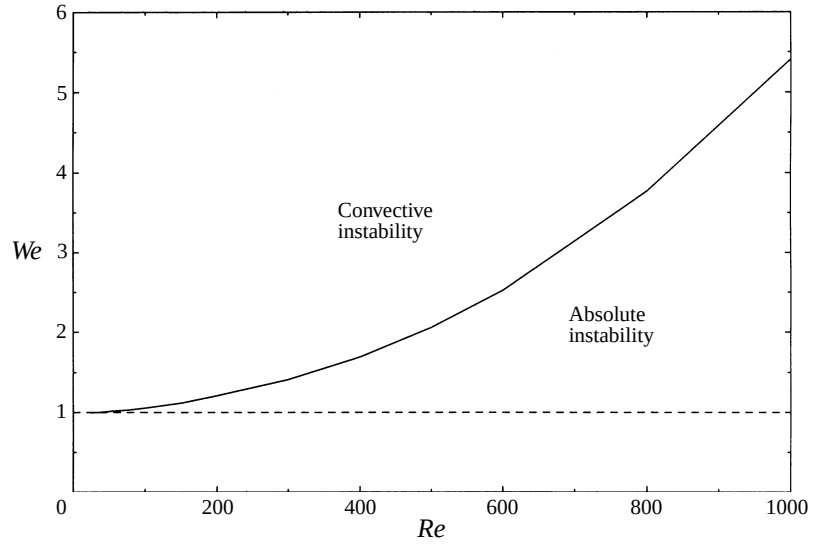


FIGURE 5. Critical Weber number for absolute instability. $Fr = 0.000340625$, $\rho_r = 0.0013$, $\mu_r = 0.017$, $l = 5$.

0.998. Emergence of a saddle point for this flow as $We$ is reduced from 0.999 to 0.998 is shown in figure 6. The dashed lines in this figure correspond to the $\omega_r = 0$ curves in figure 4, and the solid lines with smaller and larger values of $-k_i$ correspond, respectively, to the downstream amplification and the upstream decay of the convected disturbances. It is found that the transition Weber number depends only weakly on $Re$ and other flow parameters, and is approximately 1. This seems to correspond to the experimental observation of Lin & Roberts (1981) and Antoniades & Lin (1980). They found that the liquid curtain ruptures explosively at their Weber number 0.5 which corresponds to $We = 1$ in this work. Their Weber number is defined as $S/2\rho_1 U_0^2 d$. For

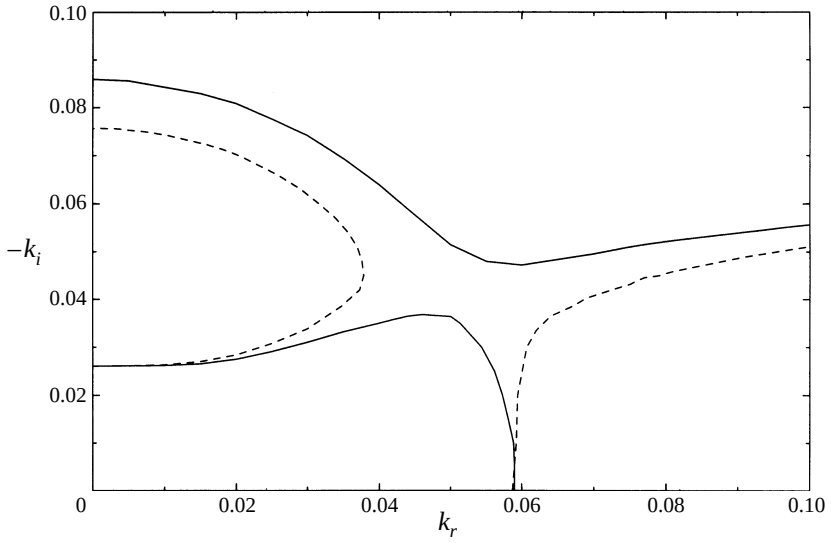


FIGURE 6. Emergence of saddle point. $Re = 52.72$, $Fr = 1.6 \times 10^{-4}$, $\rho_r = 0.0013$, $\mu_r = 0.017$, $l = 5$: ——, $We = 0.999$; – – –, 0.998.

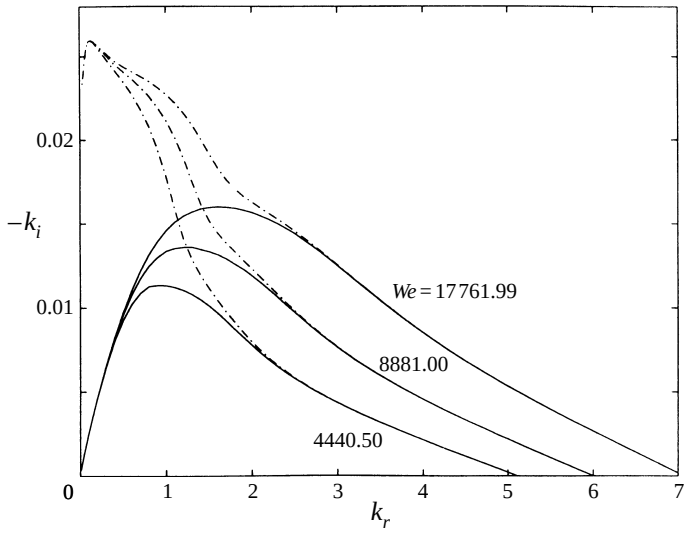


FIGURE 7. Effect of $We$ on convective instability. $Re = 15711.77$, $Fr = 3.835 \times 10^{-6}$, $\rho_r = 0.0013$, $\mu_r = 0.017$, $l = 5$: —·—, sinuous mode; ——, varicose mode.

$We > 1$, both sinuous and varicose waves were observed by them. They also found that both waves are downstream propagating, but sinuous waves have much higher amplification rates. No absolute instability was found in the previous theoretical study of Lin *et al.* (1990). They neglected the viscosity of the surrounding gas which is unbounded. Moreover the basic flow in the liquid satisfied the Navier–Stokes equations only approximately. They found that the liquid curtain is neutrally unstable rather than absolutely unstable when $We < 1$.

Although the surface tension is shown to be responsible for the absolute instability, it actually reduces the amplification rate of disturbances in the regime of convective instability when $We \gg 1$. This is shown in figure 7. It is seen that the amplification rate

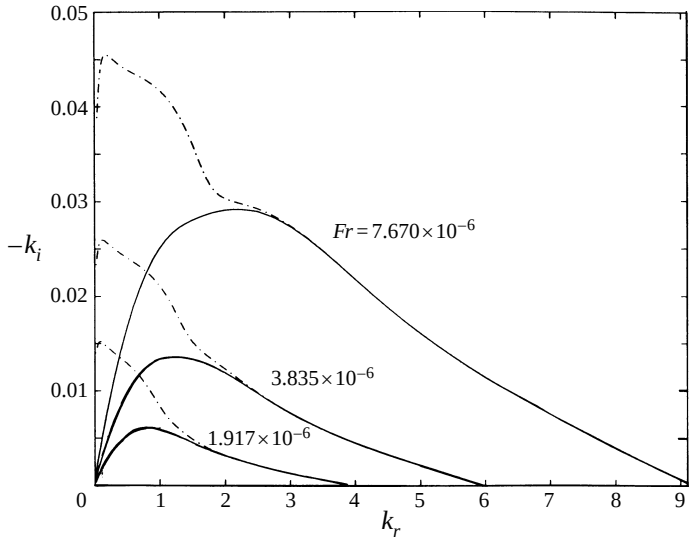


FIGURE 8. Effect of $Fr$ on convective instability. $Re = 15711.77$, $We = 8881.00$, $\rho_r = 0.0013$, $\mu_r = 0.017$, $l = 5$: —·—, sinuous mode; ——, varicose mode.

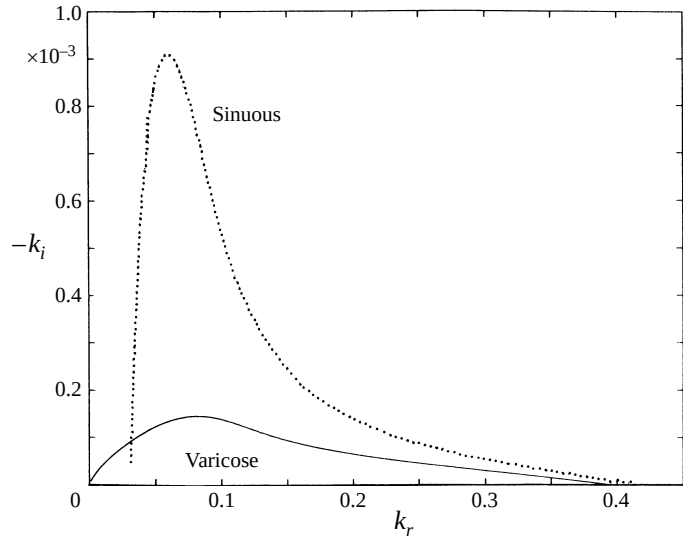


FIGURE 9. Stabilization of long sinuous waves. $Fr = 0$, $Re = 7855.89$, $\rho_r = 0.0013$, $\mu_r = 0.017$, $We = 2220.25$, $l = 5$.

of the sinuous mode is higher than that of the varicose mode. For both modes, the amplification rate as well as the cutoff wavenumber above which the disturbance is damped are reduced when the surface tension is increased. The effect of surface tension becomes relatively insignificant as $k_r \to 0$, as expected.

The effect of gravity is shown in figure 8. As the gravitational force is decreased relative to the inertial force, the cutoff wavenumber as well as the amplification rates of both sinuous and varicose modes of convectively unstable disturbance are reduced. The reduction of the amplification rate is quite significant for long sinuous waves. This suggests that the origin of long sinuous waves is the gravitational force. Figure 9 shows

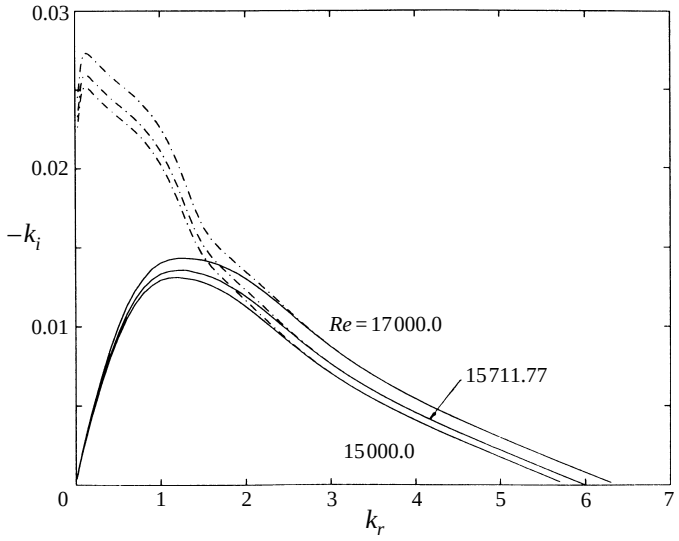


FIGURE 10. Effect of $Re$ on convective instability. $Fr = 3.835 \times 10^{-6}$, $We = 8881.00$, $\rho_r = 0.0013$, $\mu_r = 0.017$, $l = 5$: —·—, sinuous mode; ——, varicose mode.

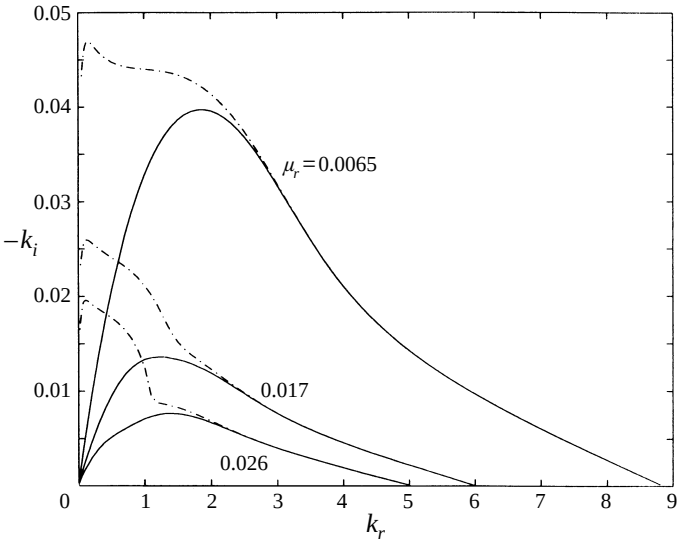


FIGURE 11. Gas viscosity reduces the amplification rate. $Re = 15711.77$, $Fr = 3.835 \times 10^{-6}$, $We = 8881.00$, $\rho_r = 0.0013$, $l = 5$: —·—, sinuous mode; ——, varicose mode.

that this is indeed the case. As the gravity vanishes, the long sinuous waves of $k_r < 0.03$ become stable. However, the varicose mode remains unstable. Nevertheless, the sinuous mode remains dominant for the rest of the unstable range of wavenumbers.

Figure 10 shows that an increase in the liquid viscosity results in a decrease in the amplification rate for the more dominant sinuous mode as well as the varicose mode. Figure 11 shows the similar effect of the gas viscosity when $\mu_r$ is varied at $Re = 15711.77$ and the rest of the parameters remain the same as those in figure 10. The enhancement of the convective instability by increasing the gas inertial force through

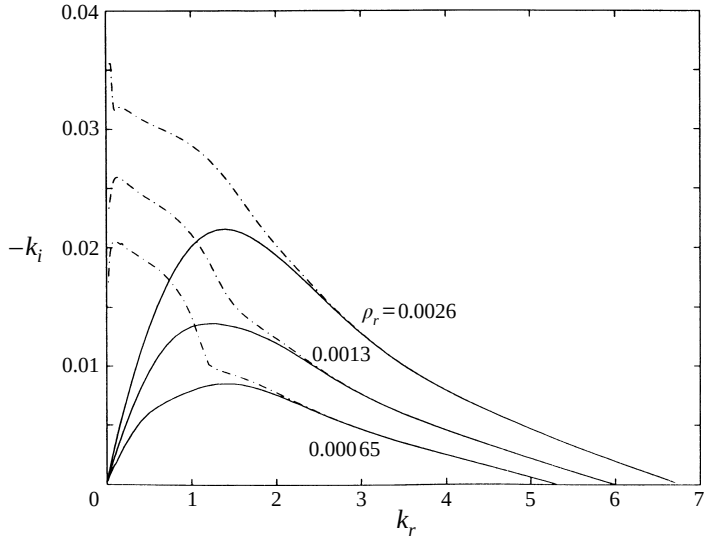


FIGURE 12. Gas density enhance the amplification rate. $Fr = 3.835 \times 10^{-6}$, $Re = 15711.77$, $We = 8881.00$, $\mu_r = 0.017$, $l = 5$: —·—, sinuous mode; ——, varicose.

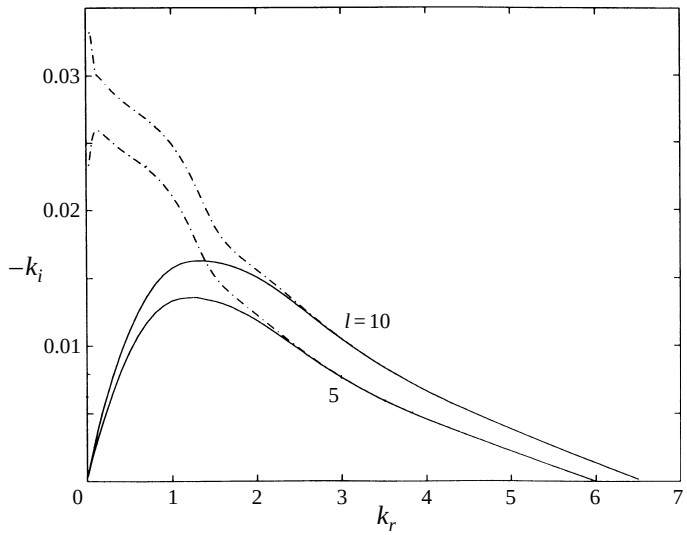


FIGURE 13. Effect of $l$ on convective instability. $Fr = 3.835 \times 10^{-6}$, $Re = 15711.77$, $We = 8881.00$, $\mu_r = 0.017$, $\rho_r = 0.0013$.

an increase in the gas density is shown in figure 12. Figure 13 shows that the amplification rate can be reduced by reducing the gap filled by gas.

The convective instability described in figures 2–13 is essentially an interfacial instability. The real and imaginary parts, $\phi_r$ and $\phi_i$, of an even sinuous mode eigenfunction as well as the corresponding Reynolds stress divided by the density in the liquid and gas flows are given in figure 14 for a water–air system defined by the flow parameters given in the caption. It is seen that most of the energy transfer through the Reynolds stress occurs near the liquid–gas interface. In a liquid–liquid system, the

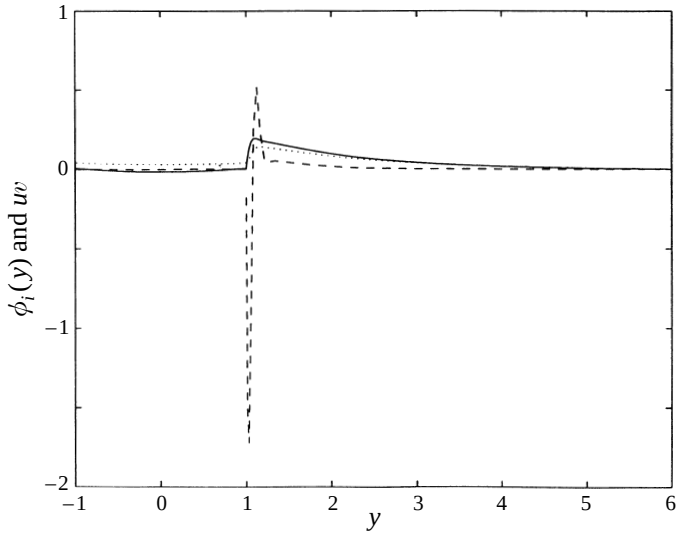


FIGURE 14. Even-eigenfunction (sinuous mode) and $uv$. $Re = 15711.77$, $Fr = 7.67 \times 10^{-6}$, $We = 8881.0$, $\rho_r = 0.0013$, $\mu_r = 0.017$, $l = 5$, $k_r = 1$, $k_i = -0.0417558$, $\omega_r = -0.00$, $\omega_i = -0.964095$. ——, $\phi_r$; ...., $\phi_i$; — — —, $uv$.

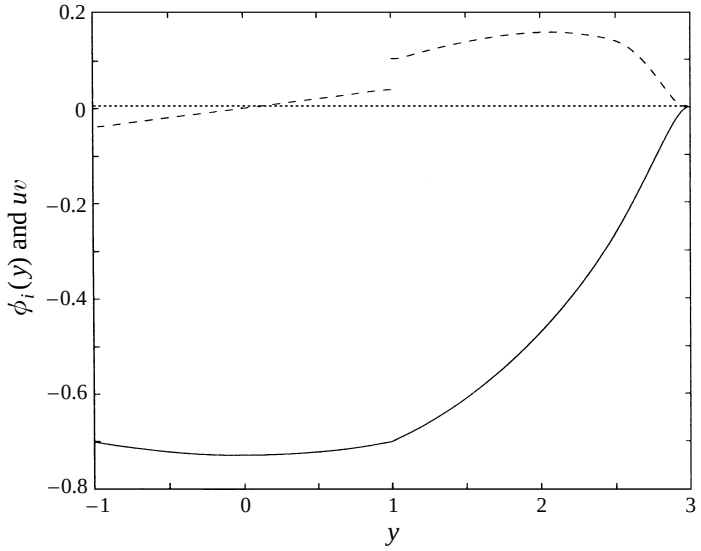


FIGURE 15. Shear waves near the wall for a sinuous mode. $Re = 3333.33$, $Fr = 10^{-5}$, $We = 10^5$, $\rho_r = 0.9$, $\mu_r = 0.6$, $l = 2$, $k_r = 0.033$, $k_i = -0.004462709\,43$, $\omega_r = 0.000$, $\omega_i = -0.075\,463\,940\,7$. ——, $\phi_r$, ...., $\phi_i$; — — —, $uv$.

situation may be quite different. Most of the energy transfer from the basic flow to the disturbances through the Reynolds stress may actually occur near the solid wall. An example is given in figure 15. It should be pointed out that the discontinuities of $uv$ at the interface appearing in figures 14 and 15 are due to the discontinuity of $u_i$ associated with $U_{i,y}$ in (5$c$).

## 5. Discussion

The critical Weber number below which the liquid sheet is absolutely unstable and above which the sheet is convectively unstable is found to be approximately 1, which varies only slightly with other flow parameters considered in computation. Hence, in the curtain coating application, the Weber number must remain larger than one in any part of the operation. It is found that the spatial growth rate of convectively unstable disturbances decreases as $\mu_r$ is increased or $\rho_r$, $Fr$, $Re$, $We$ and $l$ are decreased with the rest of the flow parameters kept constant. Therefore in order to retard on earth the convectively unstable wave packet in the curtain coating of a given liquid, one should coat at high speed in low-density high-viscosity gas surrounding the liquid in a narrow gap. The absolute and convective instability of a liquid curtain is shown to be due to the surface tension effect. It is not caused by the counterflow effect discussed by Huerre & Monkewitz. The constant thickness of the liquid sheet in the exact basic flow is maintained by adjusting the gas pressure gradient to be the same as that of the liquid sheet. If no such adjustment is made, the liquid sheet will become thinner as the liquid accelerates in the direction of gravitational acceleration. Thus the local Weber number will increase downstream for a given fluid flowing at a given flow rate $U_0 d$, since $We = \rho_1 U_0(U_0 d)/S$. For absolute instability to occur $We$ must be smaller than $We\,c$. As the local Weber number becomes larger in the downstream direction, the thinning of the liquid sheet will not promote absolute instability. For stable application of liquid curtains, therefore, one may wish to accelerate the flow in the downstream direction.

Although the theoretical condition of absolute instability coincides with the experimental condition of liquid curtain rupture at $We < 1$, the manner in which the absolute instability leads to the highly nonlinear phenomenon of rupture remains unknown. The nonlinear mechanism of direct resonance advanced by Akylas & Benney (1980) may be relevant here.

This work was supported in part by Grant no. DAAH04-93-G-0395 of ARO, and no. NAG3-14032 and no. NGT-51142 of NASA. The computation was carried out with the computer facilities at Clarkson University.

## REFERENCES

Akylas, T. R. & Benney, D. J. 1980 *Stud. Appl. Maths* **63**, 209.

Antoniades, M. G. & Lin, S. P. 1980 *J. Colloid Interface Sci.* **77**, 583.

Bers, A. 1983 *Handbook of Plasma Physics*, vol. 1, pp. 452–516. North-Holland.

Briggs, R. J. 1964 *Electron Stream Interaction with Plasmas*. MIT Press.

Brown, D. R. 1961 *J. Fluid Mech.* **10**, 297.

Clark, C. J. & Dombrowski, N. 1972 *Proc. R. Soc. Lond.* A **329**, 467.

Crapper, G. D., Dombrowski, N., Jepson, W. P. & Pyott, G. A. D. 1973 *J. Fluid Mech.* **57**, 671.

Crapper, G. D., Dombrowski, N. & Pyott, G. A. D. 1975 *Proc. R. Soc. Lond.* A **342**, 209.

Drazin, P. G. & Reid, W. H. 1985 *Hydrodynamic Stability*. Cambridge University Press.

Gottlieb, D. & Orszag, S. G. 1977 *Numerical Analysis of Spectral Methods; Theory and Applications*. CBMS-NSF Regional Conference Series in Applied Mathematics, vol. 26, SIAM, PA.

Huerre, P. & Monkewitz, P. A. 1985 *J. Fluid Mech.* **159**, 151.

Kelly, R. E., Goussis, D. A., Lin, S. P. & Hsu, F. K. 1989 *Phys. Fluids* A **1**, 819.

Kistler, S. F. & Scriven, L. E. 1984 *Intl J. Numer. Meth. Fluids* **4**, 207.

Lanczos, C. 1956 *Applied Analysis*. Prentice-Hall.

Leib, S. J. & Goldstein, M. E. 1986*a* *J. Fluid Mech.* **168**, 479.

Leib, S. J. & Goldstein, M. E. 1986*b* *Phys. Fluids* **29**, 952.
Lin, S. P. 1981 *J. Fluid Mech.* **104**, 111.
Lin, S. P. & Lian, Z. W. 1989 *Phys. Fluids* A **1**, 490.
Lin, S. P., Lian, Z. W. & Creighton, B. J. 1990 *J. Fluid Mech.* **220**, 673.
Lin, S. P. & Roberts, G. 1981 *J. Fluid Mech.* **112**, 443.
Muller, D. E. 1956 *Mathematical Tables and Aid to Computation*, vol. 10, pp. 208–230.
Orszag, S. A. 1971 *J. Fluid Mech.* **50**, 689.
Renardy, Y. 1987 *Phys. Fluids* **30**, 1638.
Rombers, S. 1984 *Problem Solving Software for Mathematical and Statistical FORTRAN Programming*. I & II. IMSL.
Taylor, G. I. 1959*a* *Proc. R. Soc. Lond.* A **253**, 289.
Taylor, G. I. 1959*b* *Proc. R. Soc. Lond.* A **252**, 296.
Taylor, G. I. 1959*c* *Proc. R. Soc. Lond.* A **253**, 313.
Taylor, G. I. 1963 *The Scientific Papers of G. I. Taylor*, vol. 3, no. 25. Cambridge University Press.
Weihs, D. 1978 *J. Fluid Mech.* **87**, 289.